apatite is mostly a few microns for without-collagen, while under the coexistence of collagen the product becomes the agglomerate of apatite crystallites of less than 100 nm with the lower crystallinity, revealed from X-ray diffraction analysis.

Failure of dental implants by bone desorption

In clinical cases of dental implants, failure sometimes occurs. Figure 5 shows the example of hydroxyapatite-coated titanium implant: before (a) and after (b) implantation. Failure occurs through inflammation and the resorption of apatite and the surrounding alveolar bone. Inflammation is induced by various reasons. The breakage of apatite-coating film or release of fine dust of apatite powders is one of the causes.

Resorption of nanoapatite and simultaneous osteogenesis in bone circumstances

When the biomimetic nanocomposites of apatite and collagen fibrils were implanted in the subcutaneous tissue, they were covered with fibrous connective tissue and then resorbed mostly at 8 weeks by phagocytosis.

Figure 6 shows the histopathological image when they were implanted in the bone marrow of rat for 8 weeks [2]. The area of nanocomposites (asterisks) was decreased and covered with new bone (white asterisks) of lamellar structures. Resorption of the nanocomposites and replacement by new bone proceeded. This tendency was progressed with time by 12 weeks. As shown in Fig. 6, phagocytosis

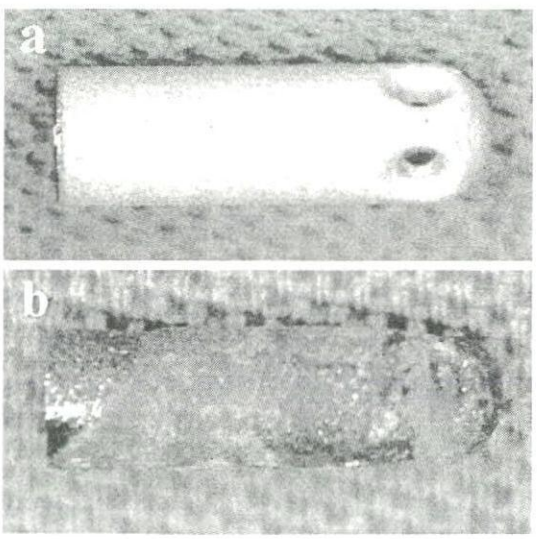

Fig. 5. Example of failure of dental implant of apatite-coated titanium: before (**a**) and after (**b**) implantation

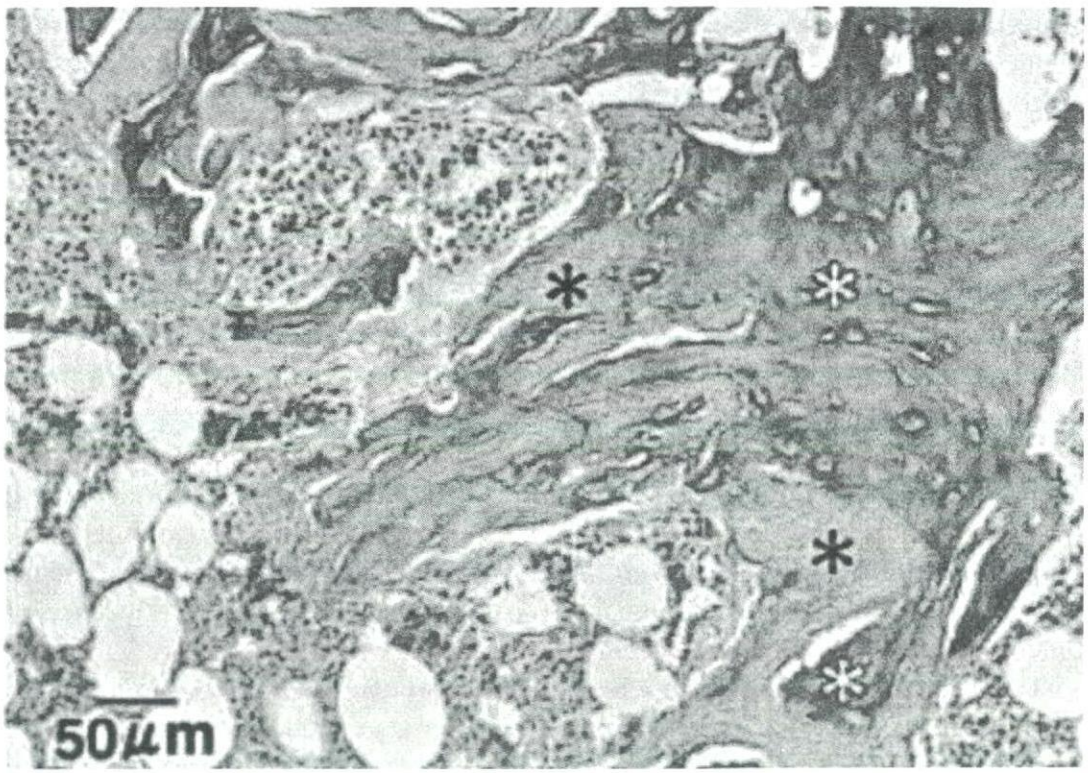

Fig. 6. Histology at 8 weeks after implantation in the bone marrow of rat. Materials (*asterisks*) were decreased and covered with new bone (*white asterisks*) with lamellar structures. AZ stain [2]

of nanoapatite by osteoclasts and osteogenesis by osteoblasts occurred adjacently to each other. Resorption and remodeling were similar to the case of autologous bone graft. As a result nanoapatite composites work as bone substitute materials for hard-tissue reconstruction.

Discussion

Nanosizing effect (general)

Nanosizing effect of materials onto living organism is usually interpreted as the aspects of the increase in specific surface area, which pronounces the chemical reactivity with the decrease in particle size. Effects related to the ionic dissolution correspond to this category, such as the acceleration of toxicity observed in Ni where tumor was generated in the long-term implantation for 0.5 μm particles [4], compared with necrosis that occurred in short term for macroscopic size [5]. There are, however, other kinds of effects [4]. Biocompatible titanium causes inflammation in abraded fine particles, when produced in the sliding parts of artificial joints, and asbestos [6], a kind of clay mineral, induces mesothelioma after a long

term, large quantity of exposure. They can be understood as the physical particle effect, apart from the chemical material properties of either toxicity or biocompatibility.

Figure 2 showed clearly the cytotoxicity due to fine particles and its size dependence. Cytotoxicity and inflammation were pronounced when the particle size was smaller than 10 μm, about the cell size, where phagocytosis was induced.

Bioactive properties induced by nanosizing

Specific surface area effect is based solely on the material properties, and material-dependent, whereas the physical particle size effect has the origin in the relative size relationship between particles and cell/tissue and independent of materials. Stimulus arises as non-specific events to any bioinert, bioactive materials of metals [7], ceramics, polymers by biological process, which induces the occurrence of functionality of body defense system.

The term "biocompatible" may be classified into two categories: "bioinert" and "bioactive". "Bioinert" may be used for the materials which give neither harmful effects nor positive functional effects. Alumina, carbon, and Ti may also be included in this category. "Bioactive" is used for the materials which induce the intrinsic functional effects of the living organism, usually in a positive sense, for example, apatite inducing osteoconductivity.

The judgment of positive or negative is based on the evaluation system in the application for human beings whether they work usefully or obstructively, and indifferent from their generation mechanism. If we enlarge the definition of "bioactive" as the potential properties to induce the intrinsic functional effects of the living organism, including both the positive and negative sense, nanosizing effect can be classified as bioactive whether it generates inflammation or osteogenesis.

Nanosizing induces the non-specific phagocytosis of particles, which gives rise to the superoxide production, cytokine emission and differentiation/activation of cells which lead to inflammation in tissue.

Nanosizing effect in apatite

In the case of apatite, nanosizing effect induces phagocytosis and leads to the apparent inflammation, which causes bone resorption in some cases like Fig. 5 and bone formation in other cases like Fig. 6, depending on the bone circumstances of these events. The former causes the failure of dental implants where the hydroxyapatite-coating film on titanium implant and the surrounding newly formed bone were resorbed. The breakage of apatite-coating film and release of fine dust of nanoapatite powders could be one reason to activate osteoclasts and other phagocytizing cells. The similar phenomena are also well known for other materials. For

example, abrasion particles produced from the sliding parts of artificial joints cause inflammation, whether material is polymer (polyethylene, etc.), metal (Ti, Co–Cr) or ceramics (alumina), and lead to osteolysis in the surrounding bone tissue, which determines the lifetime of using artificial joints.

When nanoapatite-collagen composites [2] or their derivatives reinforced with PLA or PLGA [8] were implanted into the bone defects of hard tissue, it leads apparently to the inflammation where cytokine emission and the differentiation or activation of osteoclasts and osteoblasts occur. Then the phagocytosis of nanoapatites by osteoclasts and osteogenesis by osteoblasts occur adjacently to each other, and the resorption of nanoapatite composites and new bone formation proceed simultaneously with time as shown in Fig. 6. As a result nanoapatite composites are substituted with new bone. Thus nanoapatite induces bioactive functions and works as bone substitutional. This tendency is more enhanced for carbonated hydroxyapatite. These phenomena are very similar to the bone remodeling process which occurs in natural bone.

Conversion of functions by nanosizing

Apatite in macroscopic size works as osteo-conductive but non-bone substitutional, while nano-size apatite works as bone substitutional.

Here, there is a conversion of functions of materials by nanosizing—from osteo-conductivity to bone substitutional properties in apatite.

Stimulus and bioactive properties of nanomaterials induced by biological process

Nanosizing causes the reaction of cells/tissue and stimulates to the occurrence of inflammation, which works as the stimulus in most cases. This toxicity is very weak compared with endotoxin [4]. Inflammation generates the conversion of functions leading to the bioactive functions for some cases, depending on the situation. These stimuli are different from those by specific surface effect where origin is solely from materials.

Conclusions

Synthesized hydroxyapatite, usually in macroscopic size, is osteoconductive but non-bone substitutional. Nanosizing of apatite induces bioactive reactivity to tissue where bone resorption or bone substitutional functions arise through the expression of inflammation, depending on the circumstances. Adjacent occurrence of resorp-

tion of nanoapatite composite by osteoclasts and simultaneous new bone formation by osteoblasts is very similar to the remodeling process of natural bone. Nanosizing works as a bioactive and causes inflammation, which leads to the conversion of functions through biological process such as from biocompatible to stimulative or from osteoconductive but non-bone substitute to bone substitute. Thus nanosizing of apatite is essential for hard tissue reconstruction and bone remodeling in the living organism.

Acknowledgments. The present study was performed under the support of Health and Labour Sciences Research Grants in Research on Chemical Substance Assessment from the Ministry of Health, Labour and Welfare of Japan (H18-Chemistry-General-006).

References

1. Tamura K, Takashi N, Kumazawa R, et al (2002) Effects of particle size on cell function and morphology in titanium and nickel. Mater Trans 43:3052–3057
2. Yokoyama A, Gelinsky M, Kawasaki T, et al (2005) Biomimetic porous scaffolds with high elasticity made from mineralized collagen—an animal study. J Biomed Mater Res Part B Appl Biomater 75B:464–472
3. Kumazawa R, Watari F, Takashi N, et al (2002) Effects of Ti ions and particles on cellular function and morphology of neutrophils. Biomaterials 23:3757–3764
4. Watari F, Tamura K, Yokoyama A, et al (2007) Biochemical and pathological responses of cells and tissue to micro- and nanoparticles from titanium and other materials. In: Bauerlein E (ed) Handbook of biomineralization, vol 3. Wiley-VCH, Weinheim, pp 127–144
5. Uo M, Watari F, Yokoyama A, et al (1999) Dissolution of nickel and tissue response observed by X-ray analytical microscopy. Biomaterials 20:747–755
6. Watari F, Inoue M, Akasaka T, et al (2006) Proceedings of the 6th Asian bioceramics symposium 2005, pp142–145
7. Matsuno H, Yokoyama A, Watari F, et al (2001) Biocompatibility and osteogenesis of refractory metal implants, titanium, hafnium, niobium, tantalum and rhenium, Biomaterials 22:1253–1262
8. Liao S, Wang W, Uo M, et al (2005) A three-layered nano-carbonated hydroxyapatite/collagen/PLGA composite membrane for guided tissue regeneration. Biomaterials 26:7564–7571

ナノマテリアルの生体反応
リスクと活用

亘理文夫
Fumio WATARI
北海道大学大学院歯学研究科教授

1 ナノマテリアルの2面性：リスクと高機能性

抗がん剤は，しばしばがん患部に到達する前に健常組織に吸収され副作用に働いてしまう．この欠点を回避するために，ドラッグデリバリーシステム(DDS)は，薬剤に標的患部にのみ特異的に結合する修飾基を付け血流中を移送し選択的に投与するシステムであり，ナノマテリアルの代表的なバイオ応用例として抗がん剤投与や遺伝子導入に開発が期待されている．

一方，生体親和性に優れるチタン[1]は摩耗粉[2,3]では炎症を引き起こし，粘土鉱物の1種アスベスト[4]は長期大量に被曝すると中皮腫を発症する．ここには，マクロでの材料特性は生体親和性を有していてもミクロ/ナノになると為害性に作用するという，ある種の機能性転換が見られる．こうした現象には，単にマクロで現れる材質が毒性か生体親和性かという特性とは別に，微粒子に起因する効果[5~11]が寄与していると考えられる．ナノテクノロジーの進展とともにナノ物質の開発が進行し，新しい機能性や高効率性が実現されつつあるが，一方，ナノサイズ化により化学反応は著しく促進されることから，メリット(高機能性)とともに，意図せずしてデメリット(為害性)もまた昂進されることも十分に可能性がある．ナノテクノロジーの人体へのバイオ応用には，あらかじめミクロ/ナノ微粒子の生体反応性に関する適切な理解と指針が必要である．

本稿では，材料がマクロからミクロ/ナノサイズ化(以下，ナノサイジングと総称)したときに起きる生体反応を概括する．

2 ナノサイジング効果(1)：溶出性材料と比表面積効果

毒性発現にせよ栄養摂取にせよ，材料に対する生体の反応の多くは水溶性のイオンとして溶出し体内に取込まれることから開始する．例えばフグにせよトリカブトにせよ，急性毒性を示す物質は水溶性である．ナトリウム(Na)のような1価の金属塩は一般に可溶性であり，そのため塩分は摂取過剰になりがちであるのに対し，難溶性の2価塩であるカルシウム(Ca)は摂取不足になりやすい．このように，マクロでの材料の生体適合性には溶出性(だけではない)が，大きな影響を及ぼす．この傾向はミクロ/ナノになっても変わらず，微粒子になりサイズが小さくなると比表面積は増大するから，溶解性や化学反応性は著しく増大する．

ナノサイジング効果は通常，この化学反応昂進を引き起こす比表面積増大効果で説明される．図1は溶出性で為害性を有する材料の代表例としてニッケル(Ni)を，非溶出性で親和性に富む材料の代表としてチタン(Ti)を取り上げ比較したもので，0.5μmの微粒子に対するヒト好中球の反応を走査型電子顕微鏡(SEM)像で示している．[7,8] マクロサイズの場合，皮膚接触でアレルギー性を示すNiを体内軟組織に埋入すると，Ni近傍の組織は壊死し遠隔領域

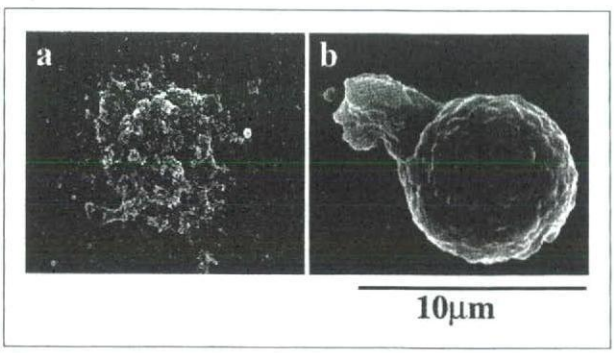

図1 0.5μm Ni(a)及び0.5μm Ti(b)微粒子に対するヒト好中球の反応(SEM像)

溶出性で為害性を有するNiでは細胞は破壊に至り，非溶出性で親和性に富むTiではその粒子サイズが貪食を誘発する．[9]

でも強い炎症を示す．こうした領域は，Niのイオン溶出領域と一致することが示される．[12] Niを0.5 μmの微粒子にし，細胞と培養液中で共在させると細胞は破壊され(図1a)，さらにラットの軟組織中に長期(半年～1年間)大量に埋入すると腫瘍を発生する．[5] この現象は，マクロでの効果がミクロ/ナノで著しく増進する比表面積効果の1例である．

3 ナノサイジング効果(2)：非溶出性材料と物理的サイズ効果

一方，マクロサイズのTiは生体親和性に優れインプラントに用いられるが，微粒子になると図1bのように貪食を誘発する．このとき，Ti粒子からのイオン溶出を誘導結合プラズマ発光分析装置(ICP-AES)で分析すると，検出限界値以下であり，イオン溶出は無視できる．[7,8] すなわち，図1bの貪食はイオン溶出という化学的効果ではなく，物理的粒子サイズそのものが貪食を誘発しているのである．

図2は，図1と同じ条件下でTi，TiO_2微粒子と共在させたヒト好中球から産生した代表的な炎症性サイトカインTNF-α量の微粒子サイズ依存性を示したものである．[5] 粒子サイズが，150～0.5 μmへ順次小さくなるにつれ放出量は増加する傾向にあるが，とりわけ10 μm以下で急激に増加する．*In vitro*, *in vivo* 試験の結果を総合すると，100 μm以上では巨視的サイズと同様の親和性を示すが，[7] 50 μm以下では刺激性が増加し，10 μm以下になると貪食作用を誘発し(図1b)，0.5～1 μm前後で最も刺激性が昂進し(図2)，炎症を引き起こす．この現象は金属，セラミックス，ポリマーの材料に依存せず，非溶出性材料やbioactive，bioinert材料共通に起きる．図2で同一サイズのTi，TiO_2粒子がほぼ同等レベルのTNF-α産生を示しているのは，その1例である．

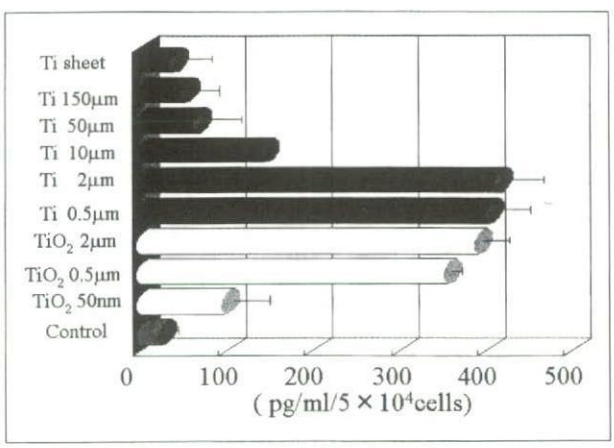

図2 炎症性サイトカインTNF-α産生のナノサイズ領域までの微粒子サイズ依存性[5]

この刺激性は細菌内毒素に比べると1/1,000～1/10,000程度であり，[13,14] 少量・短期的であれば特に問題はないと思われる．しかし大量・長期間にわたる場合には，慢性的に貪食・炎症を継続するため注意が必要である．例えば人工関節にTiを用いた場合，骨頭摺動部から発生した摩耗粉が炎症を引き起こし骨融解を導き人工関節の寿命が10年程度に終わる場合や，組成的には粘土鉱物の1種アスベストは長期大量に被曝すると中皮腫を発症する現象は，単に毒性か生体親和性かという特性や比表面積効果では理解できず，微粒子の物理的サイズ・形状が誘発し慢性的な炎症に移行する上記の刺激性が発症の背景となっている．

4 生物学的プロセスによる機能性転換

これらナノサイジングが誘発する生体反応は炎症を引き起こし，しばしばサイトカイン放出，細胞の分化誘導等の様々な生体反応のなかから，材料の置かれた状況に応じて生起した生物学的プロセスを通し，機能性転換を示現する．マクロで生体親和性を示すTiが，摩耗粉では炎症を誘発する現象やアスベストによる中皮腫発症はマクロでの親和性からミクロ/ナノでの為害性に機能性転換する例であり，さらに以下がある．

5 ナノアパタイトの骨置換性転換

アパタイトは生体親和性に富み，優れた骨伝導性を示すが，それ自体は骨に置き換わらない．そのため，インプラント材料として使用される．図3は，アパタイトコーティングチタンからなるデンタルインプラント(人工歯根)の失敗例を示したものである．[15] 親和性に優れたアパタイトといえども，微細

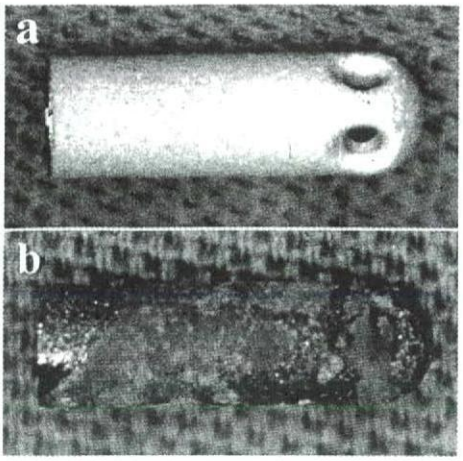

図3　アパタイトコーティングチタンデンタルインプラント

a：装着前，b：失敗例．アパタイトなどの微細なダストは貪食・炎症を誘発し，新生骨と被覆アパタイトの吸収を生じ動揺・脱落に至る．

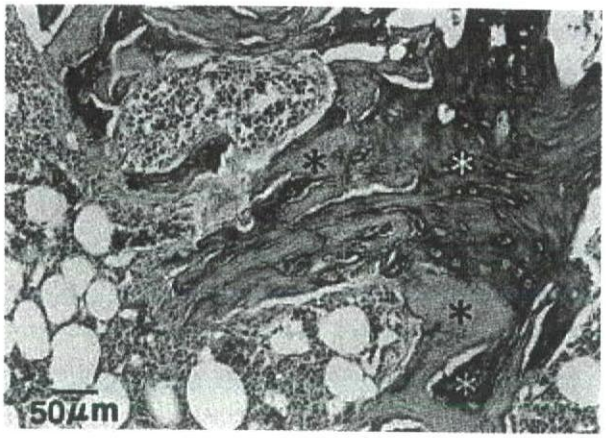

図4　ナノアパタイト–コラーゲンコンポジットの骨置換性

ナノコンポジット部(黒＊)の吸収と新生骨形成(白＊)が不可分に生じ，結果として骨置換性が達成されている．[16]

なダストを発生すると貪食・炎症を誘発し新生骨と被覆アパタイトの吸収を導き，動揺・脱落して失敗に至る．これもやはり親和性から為害性への機能性転換の例である．

しかし我々の天然骨は約50 nmのナノアパタイトからなり，リモデリングにより骨吸収と形成のプロセスを繰返している．図4は天然骨を模倣し作製したナノアパタイト–コラーゲン/コンポジットを骨欠損部に埋入した場合の組織像で，破骨細胞によるナノコンポジット部(黒＊)の吸収と骨芽細胞による新生骨形成(白＊)が同時・隣接して不可分に生じ，経時的に進行することにより結果として骨置換性が達成されている．[16] ここには，マクロにおけるアパタイトの非骨置換性からナノにおける骨置換性への機能性転換が起きている．[17]

6　カーボンナノチューブ(CNT)の細胞付着性転換

元素としての純炭素の生体適合性はNiのような為害性はないが，アパタイトのような生体活性(bioactive)やTiほどの親和性はなく，生体不活性(bioinert)と考えられる．図5は，同じ純炭素の同素体(多形)であるグラファイト(黒鉛)(a)とCNT(b)に対する骨芽細胞様細胞(Saos 2)の接着性を示したものである．結晶構造は，ともに炭素の六員環が2次元に配列したグラフェンシートからなり，マクロなグラファイトではグラフェンシートが平面状に積層しているのに対し，CNTでは単層または多

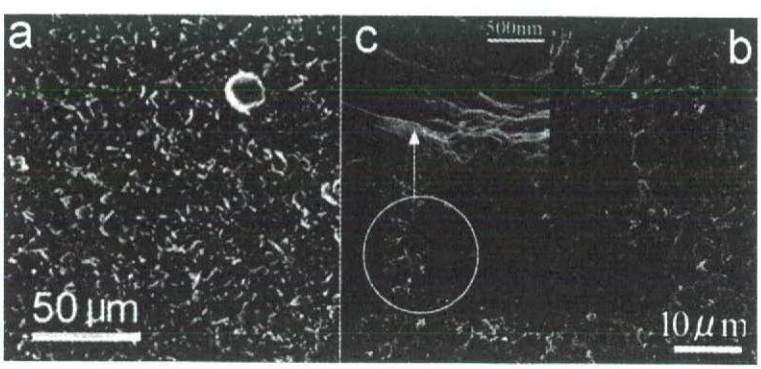

図5　グラファイト(a)とCNT(b)に対する骨芽細胞様細胞の付着性

層のグラフェンシートがナノサイズの直径の円環状に閉じたチューブ状をなしている.[18,19] グラファイト(a)には細胞がほとんど付着しないのに対し,CNT上(b)では付着・伸展し細胞末端から多数の長く延伸した直径約100 nmの糸状仮足がCNT叢と結合している(c).[20,21] 細胞非付着性のグラファイトはその抗血栓性により人工心臓弁に使用されるが,CNT上では細胞と強く付着し,ナノサイジングにより非細胞接着性から細胞接着性に機能性転換している.この強い細胞接着性の発現には,CNT表面への蛋白質吸着[20,22,23]による細胞親和性の向上と,糸状仮足が相互作用しやすい直径数nm～数10 nmのナノネットワーク構造の組成的及び幾何学的効果が寄与している.

7 ナノ微粒子の体内侵入・全身拡散と薬剤の体内動態

この材料に非特異的な物理的微粒子サイズに由来する刺激性は,マイクロメートル近傍で最大値を示した後,更に微小なナノメートル領域になるとむしろ低下する(図2).[5] ナノ物質の応用の観点からは一見都合がよさそうに見えるが,別の見方をすれば異物に対する生体の認識能力あるいは防御能力が低下するということにも通ずる.微粒子の大きさが約10 μmを切ると気管支を通過するが,図6は化粧品に使われている30 nmのTiO_2粉末をラットに強制曝露したときの体内侵入・全身分布像である.これは収束X線プローブを照射し,試料から発光した蛍光X線をマッピングするX線走査型分析顕微鏡

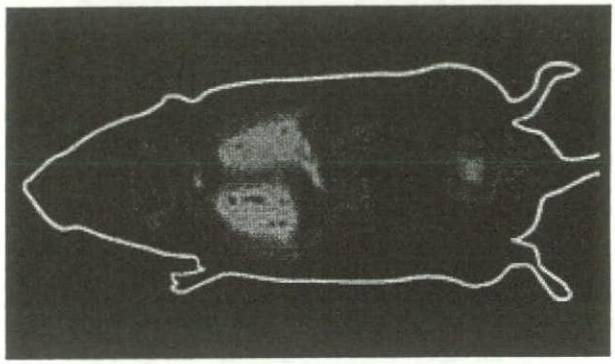

図6 呼吸器系からのナノ微粒子の体内侵入/全身拡散:30 nmTiO_2粒子の強制曝露試験後のXSAMマッピングによるラット体内の全身Ti元素分布像[5]

(XSAM)[12]により得られたTi元素分布像である.[5] 呼気に乗って肺胞に到達したナノ粒子が肺から直接血中に取り込まれ,全身に拡散することが分かる.経口投与試験でも濃度は低いが,脾臓等からTiが検出され,消化器系からも体内侵入・全身拡散することが示される.[24] これらの体内動態は,意図せずして体内侵入し為害性をなし得るというデメリットとして捉えられるが,逆の観点からいえば薬剤投与後の体内動態そのものであり,DDSの標的患部への移送プロセスというナノテクの活用のメリットとしての意義にも該当する.

図7は体内動態をより簡便に調べるために,マウスの尾静脈から直接血流に投与した結果で,XSAM-Ti元素マッピングによるTiO_2の投与直後,3時間,1日後の分布を示している.血流に乗った30 nmTiO_2粒子は,投与直後まず心臓に戻った後,肺

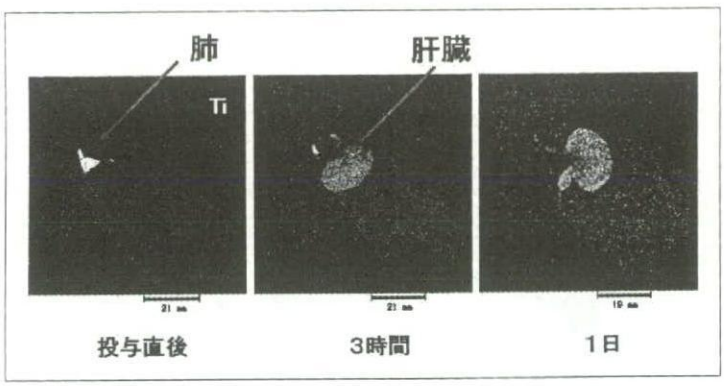

図7 XSAM-Ti元素マッピングによるマウス尾静脈注入後のTiO_2粒子(30 nm)の全身動態[24]

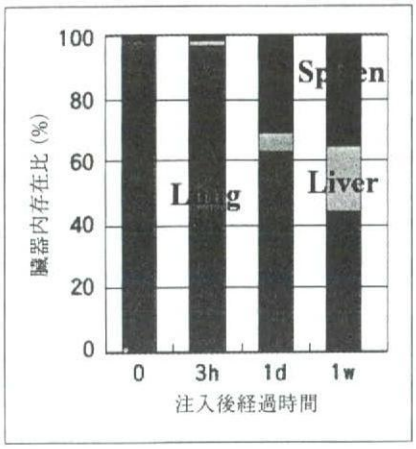

図8　TiO_2粒子の各臓器への相対的存在比の経時的変化[10]

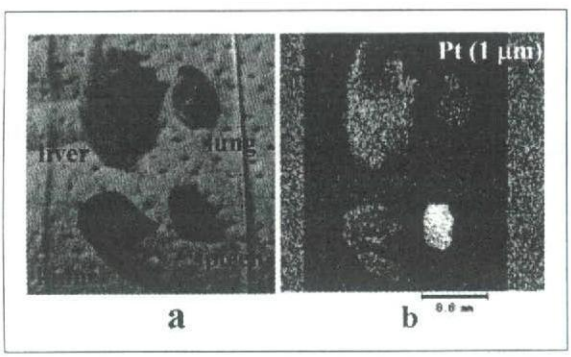

図9　Pt微粒子投与1日後のマウス各臓器(a)のPt元素マッピング像(b)[25]

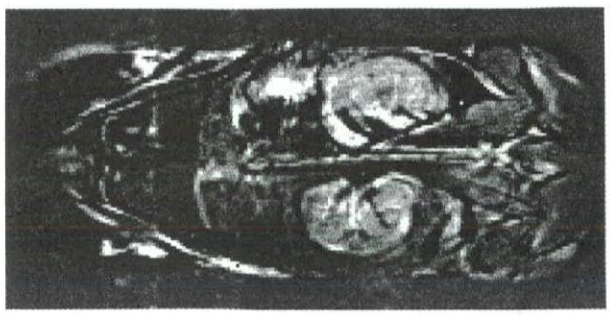

図10　マグネタイト粒子(11nm Fe_3O_4)を尾静脈注入したマウスの投与前，投与1週後のMRI差画像[25]

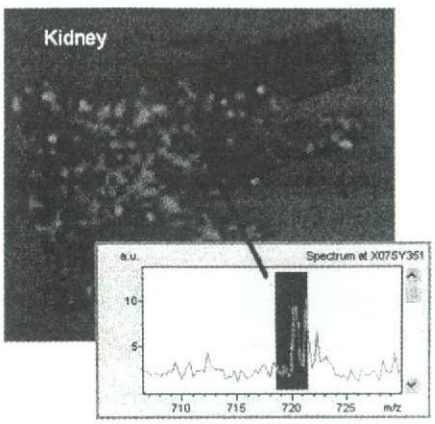

図11　水溶化フラーレン投与1時間後のラット腎臓のC_{60}レーザーマス・マッピング像(左)と，腎臓内1点からのマススペクトル(右)[25]

に到達し，数時間～数週間かけて肝臓，さらに脾臓に拡散移行する．図8はTiO_2粒子の各臓器への相対的存在比の経時的変化を示したもので，肺→肝臓→脾臓と順次臓器間移行している．[24]

図7，8のような経路を経て体内拡散するタイプの材料とは異なり，白金(Pt)微粒子では当初から脾臓に優先的に捕捉され，他の臓器に比べその後も引続き滞留している比率が高い．図9は，Pt微粒子投与1日後のマウスから摘出した各臓器のPt元素マッピング像で，脾臓で高濃度に検出され，肝臓がこれに次ぐ．

これらの臓器をICP-AESで分析し定量解析すると，各臓器中のPt濃度は脾臓で約2,000 ppm，肝臓で700 ppm，腎臓は<50 ppmとなり，また各臓器内に含まれるPt総量は体積の大きい肝臓で最も多く，初期投与量の約25%が肝臓に，次いで5%が脾臓にトラップされ，その他の臓器も含めれば40%近くが臓器で検出されたことになる．血流に乗った微粒子の相当程度が臓器に捕捉されていることが分かる．[25]

図10は，がんのハイパーサーミア治療(温熱療法)に用いられるマグネタイト粒子(11 nm Fe_3O_4)をマウスの尾静脈へ注入後，MRI撮像し画像処理により投与前，投与1週後の差画像としたもので，高濃度部が呈する白色コントラストから，腎臓への濃縮が確認できる．

図11は，レーザーアブレーション/マススペクトル(レーザー・マス)法による水溶化フラーレン投与1時間後のラット腎臓のイメージング像で，腎臓内1点からのマススペクトル(右)にはC_{60}(M=720)付近にピークが認められ，そのマッピング像(左)がフラーレンの臓器内分布を表示している．フラーレン

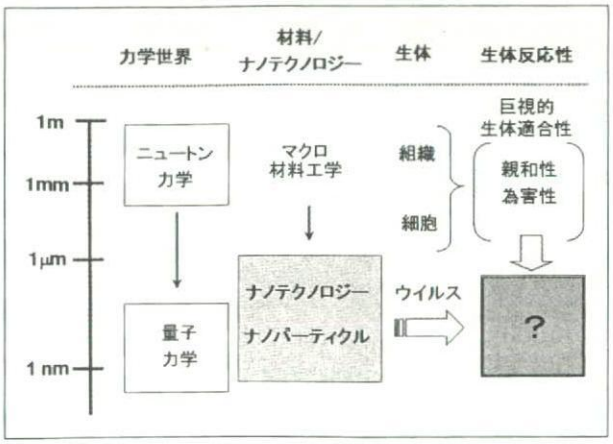

図12　ナノテクノロジーの力学世界，生体との関係及び材料のマイクロ/ナノサイジングと生体反応性の関連[6]

については血液脳関門を通過するか否かという議論があり，本方法はその判定にも有効な手段と期待される．[25]

8 おわりに

図12はナノテクノロジーの力学世界，生体との関係及び材料のマイクロ/ナノサイジングと生体反応性の関連を示したものである．[5] 比表面積増大による化学反応促進効果は材料特性のバルク(図の上方)からミクロ/ナノ(下方向)への延長であり，触媒のように同一機能が昂進する効果である．その発現は材料自体にのみ由来し，生体とは無関係に生起する．溶出性材料における比表面積効果は極めて顕著で，毒性の場合には急性で容易に認識できる．

一方，化学的溶出効果が無視し得る非溶出性材料やbioactive，bioinert材料ではマクロでは問題にならないが，おおよそ10 μm以下になると材質によらず微粒子の物理的サイズ効果による刺激性が顕現化する．物理的サイズ・形状効果は微粒子と細胞・組織との相対的なサイズの大小関係に由来し，ナノサイジングが誘発する材料–生体間(図12の横方向)の相互作用であり，これら生物学的プロセスを通して金属，セラミックス，ポリマーによらず材料に非特異的に発現する効果である．この効果により誘起された生体反応は，状況に応じ生体親和性から為害性へ，非骨置換性から骨置換性へ，細胞非接着性から細胞接着性へとマクロの物性から生物学的プロセスを通し機能性転換を生じるに至る．

ナノ微粒子は生体が防御機構の対象と想定してこなかった可能性があり，免疫システムが十分に作動せず，微粒子サイズが200 nm以下，典型的には50 nm以下になると，呼吸器系・消化器系を通して体内侵入・全身拡散を起こし得る．これは健康・環境の観点からはリスクであるが，逆にDDSのような薬剤投与の観点からは，生体防御機構による拘束を回避し体内投与に活用できる点で好都合である．ナノマテリアルは，人間の意図する目的と合致すれば高機能性というメリットとして作用するが，一方また意図せずして為害性というデメリットとして発現する可能性もある．マクロとは異なり，ナノマテリアルは本質的に高機能性と刺激性の2面性を併せ持ち，その制御が重要である．

参考文献

1) Matsuno H. *et al*., *Biomaterials*, 22, 1253–1262 (2001).
2) Tamura Y. *et al*., *Dent. Mat. J*., 21, 355–372 (2002).
3) Zhu Y., Watari F., *Dent. Mat. J*., 25, 244–252 (2007).
4) Watari F. *et al*., Proc. 6th Asian BioCeramics Symp., 2006, pp. 142–145.
5) Watari F., "Handbook of Biomineralization 3," Ed. E. Bauerlein, Wiley-VCH, Weinheim, 2007, pp. 127–144.
6) 亘理文夫，バイオマテリアル-生体材料，24，300–310 (2006).
7) Kumazawa R. *et al*., *Biomaterials*, 23, 3757–3764 (2002).
8) Tamura K. *et al*., *Mat. Trans*., 43, 3052–3057 (2002).
9) Watari F. *et al*., *J. Ceram. Soc. Jap*., 116, 1–5 (2008).
10) Watari F. *et al*., *Trans. Mat. Res. Soc. Jap*., 33, 209–214 (2008).
11) 亘理文夫，金属，78，859–862 (2008).
12) Uo M., *Biomaterials*, 20, 747–755 (1999).
13) Kiura K. *et al*., *J. Biomed.Nanotech*., 1, 359–364 (2005).
14) Sato Y. *et al*., *Mol. BioSystems*, 1, 176–182 (2005).
15) Watari F. *et al*., *Composit. Sci. Tech*., 64, 893–908 (2004).
16) Yokoyama A. *et al*., *J. Biomed. Mater. Res*：*Appl. Biomater*., 75, 464–472 (2005).
17) Watari F. *et al*., "Interface Oral Health Science 2007," Ed. Watanabe M., Okuno O., Springerpp, Japan, 2008, pp. 139–147.
18) Ushiro M. *et al*., *Phys. Rev. B*, 73, 144103/1–11 (2006).
19) Yokoyama A. *et al*., *Nano Let*., 5, 157–161 (2005).
20) Aoki N. *et al*., *Dent. Mat. J*., 26, 178–185 (2007).
21) Aoki N. *et al*., *Chem. Let*., 35, 508–509 (2006).
22) Akasaka T. *et al*., *Mat. Sci. Eng. C*, 26, 675–678 (2005).
23) Li X. M. *et al*., *J. Biomed. Mater. Res. A*, (2008), DOI：10.1002/jbm.a.32203.
24) Watari F. *et al*., *Bioceramics*, 20, (*Key Engineering Materials*, 361–363), 95–98 (2007).：Trans. Tech. Publ.
25) 亘理文夫(編)，厚生労働科学研究補助金化学物質リスク研究事業，ナノ微粒子の体内動態可視化法の開発，平成19年度総括・分担研究報告書，2007，pp. 1–168.

Key Engineering Materials Vols. 396-398 (2009) pp 569-572
online at http: www.scientific.net

Online available since 2008/Oct/21

Visualization of invasion into the body and internal diffusion of nanoparticles

F.Watari[1, a], S.Abe[1], I.D.Rosca[2], A.Yokoyama[1], M.Uo[1], T.Akasaka[1], N.Takashi[1], Y.Totsuka[1], E.Hirata[1], M.Matsuoka[1], K.Ishikawa[1], S.Itoh[1] and Y.Yawaka[1]

[1]Graduate School of Dental Medicine, Hokkaido University, Sapporo 060-8586, Japan

[2]Mechanical & Industrial Engineering, Concordia University, Montreal, Quebec H3G1M8, Canada

[a]watari@den.hokudai.ac.jp

Keywords: nanoparticle, internal diffusion, nanotoxicology, size effect, DDS, mapping.

Abstract. Nanoparticles may invade directly into the internal body through the respiratory or digestive system and diffuse inside body. The behavior of nanoparticles in the internal body is also essential to comprehend for the realization of DDS. Thus it is necessary to reveal the internal dynamics for the proper treatments and biomedical applications of nanoparticles. In the present study the plural methods with different principles such as X-ray scanning analytical microscope (XSAM), MRI and Fluorescent microscopy were applied to enable the observation of the internal diffusion of micro/nanoparticles in the (1) whole body level, (2) inner organ level and (3) tissue and intracellular level. Chemical analysis was also done by ICP-AES for organs and compared with the results of XSAM mapping.

Introduction

Particles of the size below 200nm may invade directly into the internal body through the respiratory or digestive system and diffuse inside body. Nanoparticles might be the objects whose existence has not been assumed by living body defense system [1]. Thus the visualization of the internal dynamics of nanoparticles is essential for the proper treatments based on risk assessment and biomedical applications such as DDS (Drug delivery System). In the present study plural methods with different principles were applied to enable the observation of the internal diffusion of micro/ nanoparticles in the (1) whole body level, (2) inner organ level and (3) tissue and intracellular level.

Materials and Methods

1. Visualization of Internal Particle Diffusion in the Whole Body Level. The compulsory exposure test to the respiratory system was performed to rats using 30 nm TiO_2 particles. The uptake of nanoparticles through the digestive system was also tested for mice by mixing agar gelatin containing 30 nm TiO_2 particles to their foods. To inspect internal diffusion more simply, the experiments were done for mice by injecting nanoparticles directly into the cardiovascular system at caudal vein. The observation of internal distribution of nanoparticles was conducted for the whole body and each organ by elemental mapping in air using X-ray Scanning Analytical Microscope (XSAM: Horiba XGT-2000V, Tokyo, Japan) without staining [2,3]. The experiments were also done for the particles Ti, Fe, Ni, Pt, TiC, Fe_3O_4, Fe_2O_3 and carbon nanotubes [4,5]. Chemical analysis was done by ICP-AES (Inductively Coupled Plasma - Atomic Emission Spectrometry) for organs and compared with the results of XSAM mapping.

Three-dimensional and chronological observation by MRI (Magnetic Resonance Imaging) was done for the 11 nm magnetite Fe_3O_4 particles, using the MRI with the magnetic field strength 7 Tesla for animal experiment (Varian Co.Lmd) under the conditions of TR/TE 5000/20 ms, matrix 256 x 128, FOV 80 x 40 mm^2, slice thickness 1mm. The results were compared with those taken by XSAM.

2. Visualization in the Inner Organ Level. Fluorescent microscopic method was also applied to detect the internal distribution using the fluorochrome-labeled particles. The fluorescent dye,

coumarin 6, - labeled polylactic acid particles of the size about 1 μm were prepared by adding the mixture of the particles and the coumarin 6 in Ch_2Cl_2 into the 0.25% polyvinyl alcohol aqueous solution under ultrasonication. The fluorescent image from each organ was obtained. The distribution inside the organ was also inspected by elemental mapping using energy dispersive X-ray spectroscopy (EDS) installed to SEM.

3. Visualization in the Tissue and Intracellular Level. Histological and ultrastructural investigations were carried out by optical and transmission electron microscopy (OM, TEM) for the specimens prepared by ordinary process [6].

Results

1. XSAM elemental detection. Fig.1 is the XSAM elemental analysis of spleen after 10 days of oral administration of 30nm TiO_2 particles to a mouse. Although the peak height is small compared with Fe-Kα peaks around 6.5keV and those of incident X-ray beam from Rh target below 4keV, Ti-Kα peak undoubtedly exists. This confirms the phenomenon that nanoparticles were taken into the internal body through digestion system. The uptake of 30nm TiO_2 particles through the respiratory system and diffusion into the whole body was also confirmed.

2. Microscopic observation of fluorescence-labeled particles. Fig.2 is the fluorescent microscopic image of spleen at 1 week after injection of 1 μm particles of coumarin 6-labeled polylactic acid to caudal vein. Fluorescent spots are visible to be distributed all over the spleen. Judging from the spot size around 1 μm, each spot looks corresponding to a single particle. The particles of polylactic acid seem to have little tendency to coagulate. The distribution of fluorescent spots are also found in the lung and livers. They might diffuse rather dispersedly and result in being trapped in the relevant organs.

3. MRI imaging of magnetic nanoparticles. Fig.3 is MRI image before and after injection of 11 nm magnetite Fe_3O_4 particles to caudal vein. These particles are fabricated for the optimum performance of hyperthermia therapy to cancer. Due to the contrast darkened by magnetism of Fe_3O_4 particles, the comparison of images before and after injection verifies the contrast change occurred in the liver, indicating the enrichment of Fe_3O_4 particles. The similar change was observed in the spleen and kidney.

4. XSAM elemental mapping. Fig.4 is the change of XSAM Ti mappings of internal distribution of 30 nm TiO_2 particles in the body of mouse with time after injection to caudal vein. TiO_2 nanoparticles diffuse to the lung just after injection from caudal vein, then with time course to the liver and further to the spleen, which is not shown here. The following time sequence of XSAM Ti mapping shows the decrease in the lung and the increase in the liver. It takes longer time for the increase in the spleen.

Fig.5 is the XSAM Pt mapping of the lung, liver, spleen and kidney at 1 day after injection of 1 μm Pt particles to caudal vein. The Pt concentration is the highest in the spleen, followed by the liver.

5. Chemical analysis of particles contained in organs. Fig.6 shows the ICP-AES chemical analysis of total Pt content detected from each organ shown in Fig.5 at 1 day after injection. The Pt concentration in each organ was also analyzed and agreed with the results obtained by XSAM analysis of Fig.5. The total Pt content is the largest in the liver, then spleen and slight in the kidney. Although the concentration is the highest in the spleen, the total content is the largest in the liver because of the large volume.

Discussion

In the present study we used the plural methods based on the different principles to enable the visualization of internal diffusion of particles.

XSAM forms the convergent X-ray probe of 100 – 10 μm, irradiates the specimen, detects the emitted fluorescent characteristic X-ray and makes elemental mapping image as well as transmission X-ray image for the sectioned specimens. Visualization of distribution for the large

scale around 100 mm such as the full body size of rat (Fig.4) is possible in air with the high sensitivity of about 100 ppm and the spatial resolution of probe size100 – 10 μm. The comparison of XSAM mapping image (Fig.5) with the quantitative chemical analysis using ICP-AES (Fig.6) verifies the detectable concentration at 100 ppm level. This method could show the time sequence of particle diffusion from organ to organ [7].

MRI can perform the three-dimensional observation, make the horizontal or vertical image at any section as animal alive and trace the change with time using the same animal. However MRI utilizes the change of image contrast by magnetism, therefore the applicable particles are limited to the magnetic or magnetism-labeled materials. In the present study the 11 nm magnetite Fe_3O_4 particles fabricated for hyperthermia therapy against cancer were used. The results were more or less in agreement with those obtained by XSAM method.

Other than XSAM, we also used the Laser Ablation / Mass Spectroscopy Method, which analyzes mass by TOFMS (Time of Flight Type Mass Spectrometer) after the target is evaporated by laser irradiation and make two-dimensional distribution image of the desired mass. This is especially valuable for the materials composed of carbon as main constituent such as pure carbon of fullerenes, carbon nanotubes or carbon compounds of saccharides and proteins, since elemental analysis such as XSAM cannot distinguish these from tissue composed of C, N, O, H.

Conclusions

Particles cause different reaction to cell/tissue depending on their size [8,9]. This physical size effect is pronounced for less than 10 μm and causes stimulus by biological process of phagocytosis in cell and inflammation in tissue [1]. When the particle size becomes in the level of 50nm or less, they become less stimulative and the recognition by body defense system becomes weaker. The invasion of nanoparticles into the body and internal diffusion occurs for this range of particle size [10]. The present study could successfully make the visualization of internal diffusion of particles by different methods. The informations obtained here contribute to both risk assessement of nanoparticles and drug delivery path of DDS.

Acknowledgements

Research supported by Health and Laybour Sciences Research Grants in Research on Chemical Substance Assessment of Ministry of Health, Laybour and Welfare of Japan (H18-Chem-General-006).

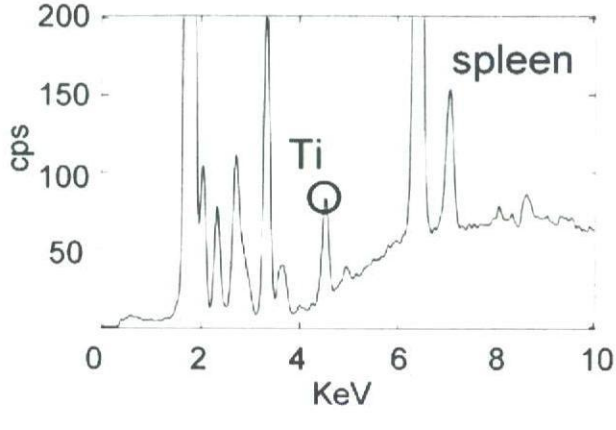

Fig.1 XSAM elemental analysis of spleen after 10 days of oral administration of 30nm TiO_2 particles

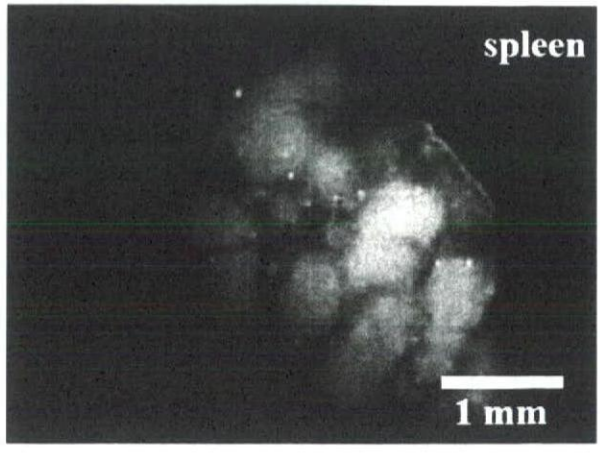

Fig.2 Fluorescent microscopic image of spleen at 1 week after injection of 1 μm particles of coumarin 6- labeled polylactic acid to caudal vein.

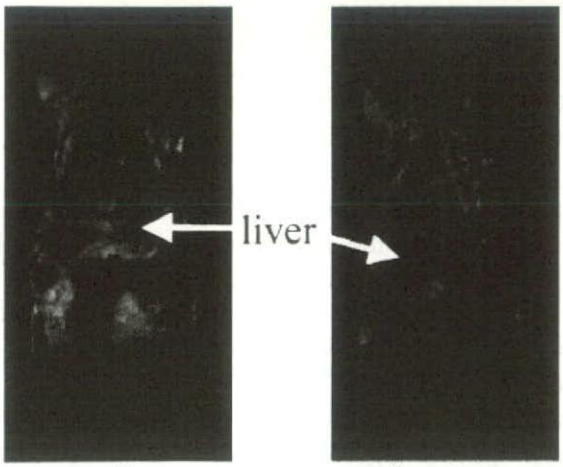

Fig.3 MRI image before and after injection of 11 nm Fe_3O_4 particles to caudal vein

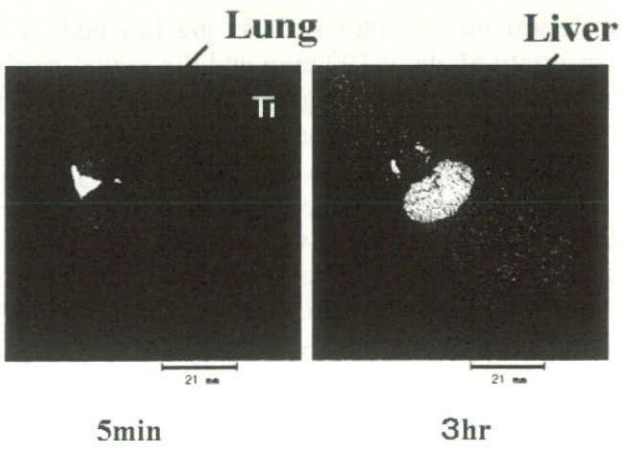

Fig.4 XSAM Ti mapping of internal distribution of 30 nm TiO_2 particles after injection to caudal vein

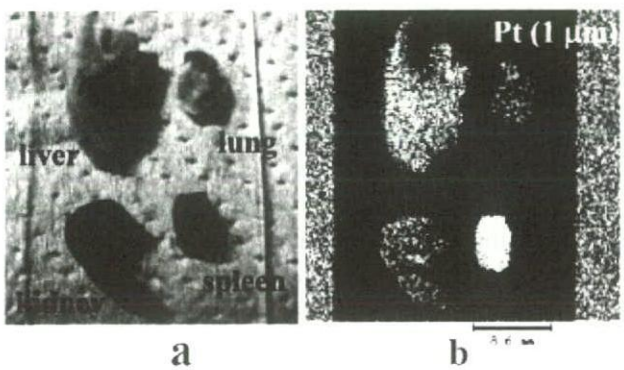

Fig.5 XSAM Pt mapping of each organ at 1 day after injection of 1 μm Pt particles to caudal vein.

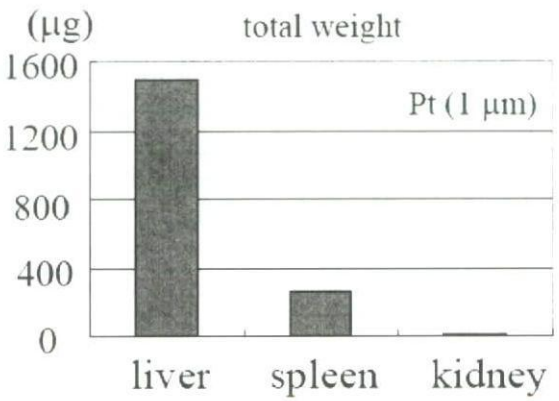

Fig.6 ICP-AES chemical analysis of Pt element contained in each organ shown in Fig.5

References

[1] F.Watari, K.Tamura, A.Yokoyama, K.Shibata, T.Akasaka, B.Fugetsu, K.Asakura, M.Uo, Y.Totsuka, Y.Sato, K.Tohji: Handbook of Biomineralization, Vol.3, Ed.E.Bauerlein, Wiley-VCH, Weinheim, p.127-144 (2007)

[2] M.Uo, F.Watari, A.Yokoyama, H.Matsuno, T.Kawasaki: Biomaterials 20(1999), 747-755

[3] M.Uo, M.Tanaka, F.Watari: J.Biomed.Mater.Res.Part B:Appl.Biomater. 70B(2004), 146-151

[4] M.Ushiro, K.Uno, T.Fujikawa, Y.Sato, K.Tohji, F.Watari, W.Chun, Y.Koike, K.Asakura: Phys. Rev. B 73, 144103/1-11(2006)

[5] Aoki N, Akasaka T, Watari F, Yokoyama A, *Dent.Mat.J.*, 26 (2007) 178-185

[6] A.Yokoyama, Y.Sato, Y.Nodasaka, S.Yamamoto, T.Kawasaki, M.Shindoh, T.Kohgo, T.Akasaka, M.Uo, F.Watari, K.Tohji: Nano Letters 5 (2005) , 157-161

[7] F.Watari, S.Abe, C.Koyama, A.Yokoyama, T.Akasaka, M.Uo, M.Matsuoka, Y.Totsuka, M.Esaki, M.Morita, T.Yonezawa: J.Cera.Soc.Jap., 116 (1) , 1-5, 2008

[8] R.Kumazawa, F.Watari, N.Takashi, Y.Tanimura, M.Uo, Y.Totsuka: Biomaterials 23(2002), 3757-3764

[9] K.Tamura, N.Takashi, R.Kumazawa, F.Watari, Y.Totsuka: Mat.Trans. 43(2002), 3052-3057

[10] F.Watari, S.Abe, K.Tamura, M.Uo, A.Yokoyama, Y.Totsuka: Bioceramics Vol.20 Part 1, (Key Engineering Materials Vols.361-363), Trans.Tech.Publ., p.95-98, 2007

Front. Mater. Sci. China
DOI 10.1007/s11706-009-0034-z

RESEARCH ARTICLE

Proliferation of osteoblast cells on nanotubes

F. WATARI (✉), T. AKASAKA, Xiaoming LI, M. UO, A. YOKOYAMA

Graduate School of Dental Medicine, Hokkaido University, Sapporo 060-8586, Japan

Abstract Carbon nanotubes (CNT) have a unique structure and feature. In the present study, cell proliferation was performed on the scaffolds of single-walled CNTs (SWCNT), multiwalled CNTs (MWCNT), and on graphite, one of the representative isomorphs of pure carbon, for the sake of comparison. Scanning electron microscopy observation of the growth of osteoblast-like cells (Saos2) cultured on CNTs showed the morphology fully developed for the whole direction, which is different from that extended to one direction on the usual scaffold. Numerous filopodia were grown from cell edge, extended far long and combined with the CNT meshwork. CNTs showed the affinity for collagen and proteins. Proliferated cell numbers are largest on SWCNTs, followed by MWCNTs, and are very low on graphite. This is in good agreement with the sequence in the results of the adsorbed amount of proteins and expression of alkaline phosphatase activity for these scaffolds. The adsorption of proteins would be one of the most influential factors to make a contrast difference in cell attachment and proliferation between graphite and CNTs, both of which are isomorphs of carbon and composed of similar graphene sheet crystal structure. In addition, the nanosize meshwork structure with large porosity is another property responsible for the excellent cell adhesion and growth on CNTs. CNTs could be the favorable materials for biomedical applications.

Keywords carbon nanotube, scaffold, osteoblast, regeneration, nanomaterial

1 Introduction: Two isomorphs of carbon–graphite and CNT

Carbon nanotubes (CNT) [1,2] have attracted much attention due to their unique feature in the application in the electronic and chemical fields. Recent derivatives of CNTs with different structures and compositions have been synthesized and discovered [3]. Nanomaterials [2–9] and nanocomposites [10–15] may have various effects on living organisms. In this study, a fundamental study for biomedical application, cell proliferation was performed on various nanotubes (NT), including (1) single-walled CNTs (SWCNT), (2) multiwalled CNTs (MWCNT), and on graphite, an isomorph of CNT, as a comparison.

Figure 1 shows the schematic figures of two different crystal structures of carbon: graphite and CNT. Graphite has the layer-by-layer laminated structure of flat graphene sheets, composed of C six-membered rings, whereas CNT is made of folded tubes of either single or multiple graphene sheets. Both graphite and CNTs are composed of graphene sheet and hydrophorbic characters. As element, carbon (C) would be bioinert. Graphite is used as an artificial heart valve due to its antithrombogenicity for biomedical applications. There have not been so many studies on CNTs, about their biological effects and biomedical applications [2,3,7–9,15–24]. In the present study, to evaluate the properties of CNTs in the aspects of biomedical nature, cell proliferation was performed on the scaffolds of SWCNTs and MWCNTs, and compared with that on graphite. Their features and the difference of properties are then discussed.

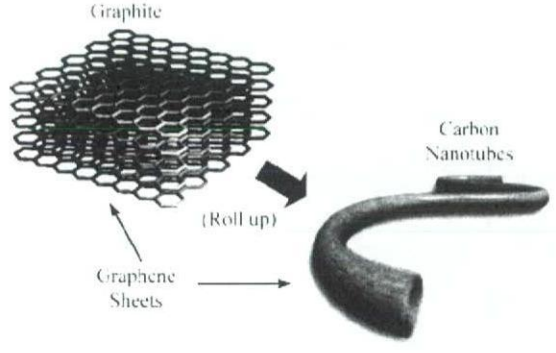

Fig. 1 Schematic figures of two different crystal structures of carbon, graphite and CNT

Received December 3, 2008; accepted January 9, 2009

E-mail: watari@den.hokudai.ac.jp

2 Materials and methods

SWCNTs of 0.9–1.5 nm diameter and 2–3 μm length synthesized by the arc discharge method with a purity of 90% (Meijo Nano Carbon Co., LTD.) and MWCNTs of 5–20 nm diameter and 20–40 μm length synthesized by the chemical vapor deposition technique with a purity of 98% (NanoLab Inc., MA USA) were used. In some cases CNTs were purified by the removal of metal particle catalysts such as Ni, Fe using acid agents and amorphous carbon by heating in air. By these treatments [3,7] CNTs got some hydrophilicity. Various NT scaffolds were made by vacuum filtration of the dispersed NT slurry onto porous polycarbonate membranes (PC) [18–20].

Human osteoblast-like cells (Saos2) were used for cell culture on NTs. Cell culture was done in Dulbecco's modified Eagle's medium (SIGMA) with 10% fetal bovine serum (Biowest) in the usual process. The morphology of cells was observed by optical microscopy, confocal laser scanning microscopy, and scanning electron microscopy (SEM). The number of cells was counted from the SEM micrographs of those attached to each scaffold, since the detachment of cells from scaffold by tripsin could not be applied for CNT scaffolds. The adsorbed amount of proteins on each scaffold was measured by the BCA method after immersion in the cell culture medium for 24 h. Alkaline phosphatase (ALP) activity was measured with LabAssay ALP (Wako, Japan) for the cells cultured on each scaffold [18].

3 Results

3.1 Cell proliferation on graphite and CNTs

Figure 2 shows the SEM image of osteoblast-like Saos2 cells cultured on graphite and MWCNT for 7 d. Very few cells were attached on graphite, while many cells were on CNTs.

Figure 3 shows the number of Saos2 cells cultured on the scaffolds of polycarbonate, graphite, MWCNT, and

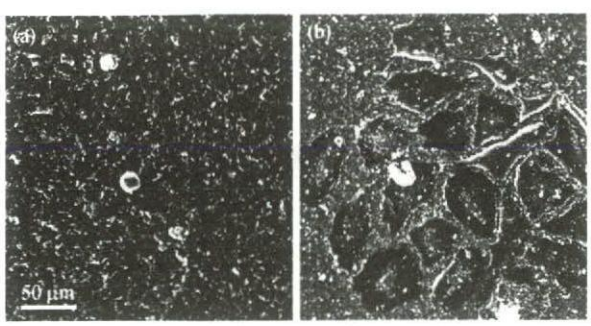

Fig. 2 SEM image of osteoblast-like Saos2 cells cultured on **(a)** graphite and **(b)** MWCNT scaffolds for 7 d

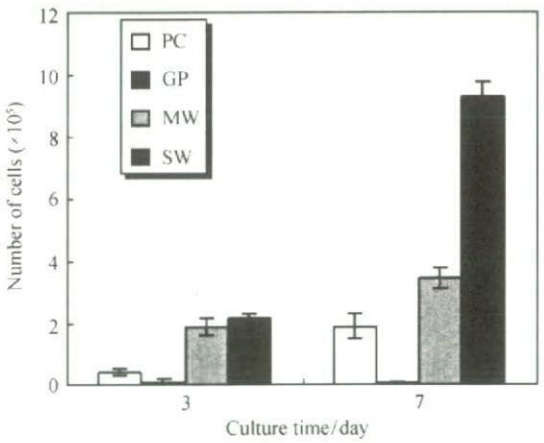

Fig. 3 Number of Saos2 cells cultured on the scaffolds of polycarbonate, graphite, MWCNT, and SWCNT for 3 and 7 d [18]

SWCNT for 3 and 7 d [18]. The cell numbers were increased with culture time. However, cell number remained nearly null on graphite. The cell numbers were largest on SWCNTs among the four scaffolds, followed by MWCNTs.

Osteoblast-like cells are usually grown in a spindle shape ~~as in Fig. 2(a)~~. On CNT scaffold, cells are grown fully to the whole direction [Fig. 2(b)] [18–20]. Figure 4 shows the SEM observation of filopodia grown from the periphery of osteoblast-like cells on the polycarbonate and MWCNT scaffolds. It is noted that numerous filopodia are extended far from cell edge onto CNTs (Fig. 5). They are mechanically combined with CNT meshwork. When tripsin, usually used to detach cells for cell number counting, was applied, cells were going to detach and float up, but could not be separated from the scaffold due to the mechanical binding of filopodia with CNTs. These results show the high cell adhesiveness of CNTs.

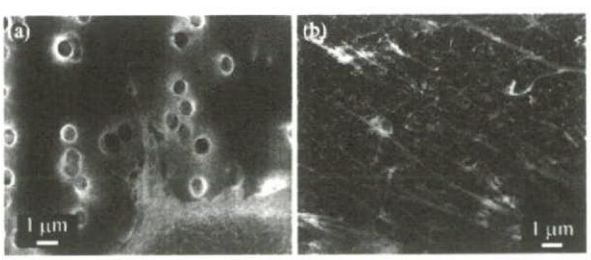

Fig. 4 SEM observation of filopodia grown from the periphery of osteoblast-like cells on **(a)** polycarbonate and **(b)** MWCNT scaffolds

3.2 Biomimetic coating of hydroxyapatite on CNT

Figure 6 is the SEM image of CNTs after immersion in simulated body fluid (SBF) for 2 weeks. Apatite was precipitated on CNT agglomeration [21,22]. This kind of

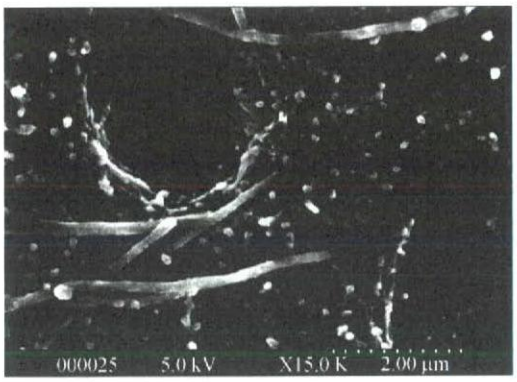

Fig. 5 SEM image of dentin surface etched with phosphoric acid after being immersed in CNT mixed solution

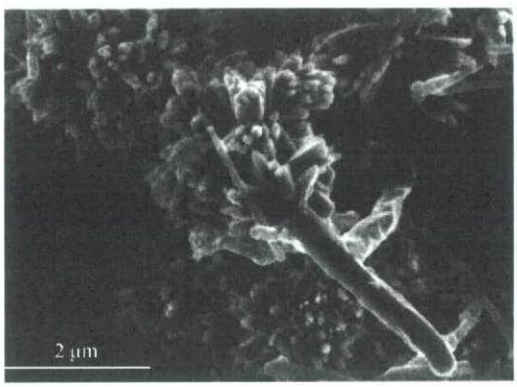

Fig. 6 SEM image of CNTs after immersion in SBF for 2 weeks

precipitation of calcium phosphate by immersion in SBF is known as the so-called biomimetic coating, which occurs typically on titanium (Ti) to form the calcium phosphate layer on its surface. This process is one of the reasons for the excellent biocompatibility of Ti, which may also be the case for CNTs.

3.3 Adsorption of CNTs onto collagen fibrils on dentin

In the treatment of dentistry for composite resin restoration, teeth are pretreated with an acid etching agent such as phosphoric acid and citric acid to enhance the interlocking effect between teeth and composite resin. When the sectioned teeth are pretreated with acid etching agent and immersed in the CNT mixed solution, the inner area of the teeth, dentin, looks black, while enamel remains white. Without acid etching dentin remains white. SEM observation reveals the adsorption of CNTs on dentin and no adsorption on enamel. Figure 5 is the enlarged SEM image of dentin surface etched with phosphoric acid after being immersed in CNT mixed solution. Dentinal tubules are observed. Collagen fibrils are exposed all over the dentin surface due to demineralization by acid etching. CNTs (long fibers) are found to be adsorbed to collagen fibrils exposed on dentin surface by acid etching. The fact that CNTs are adsorbed only on dentin but not on enamel suggests the nonspecific affinity of CNTs to proteins.

3.4 Adsorption of proteins on CNTs

Figure 7 shows the adsorbed amount of proteins on the scaffolds of polycarbonate, graphite, MWCNT, and SWCNT when immersed in the cell culture medium for 24 h [18]. The adsorbed protein amount level is very low for graphite, and is highest for SWCNT, followed by MWCNT.

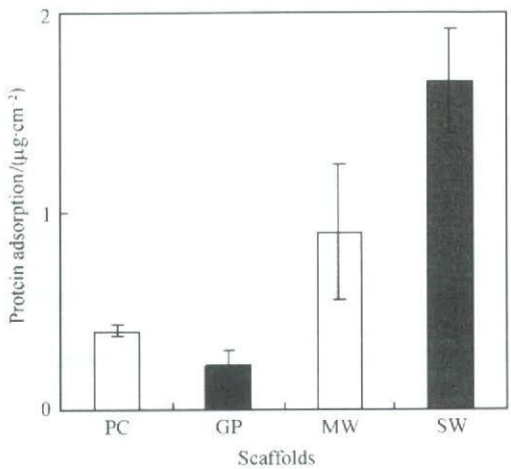

Fig. 7 Adsorbed amount of proteins on the scaffolds of polycarbonate (PC), graphite (GP), MWCNT (MW), and SWCNT (SW) in cell culture medium after 24 h [18]

3.5 ALP activity of osteoblast-like cells on CNTs

Figure 8 is the expression of total ALP activity from osteoblast-like cells cultured on the scaffolds of polycarbonate, graphite, MWCNT, and SWCNT for 3 and 7 d [18]. The degree of expression increases with culture time. It remains very low for graphite, while it increases remarkably in CNTs, the most in SWCNTs, then MWCNTs.

4 Discussion: Factors that make a difference in biological effect between graphite and CNTs

Graphite and CNTs are isomorphs of carbon and are composed of similar graphene sheet crystal structures (Fig. 1). Although the element carbon is bioinert, graphite and CNTs make a contrast difference in cell attachment and proliferation.

The present study showed the very low osteoblast cell attachment and proliferation on graphite. This is one of the properties inducing antithrombogenicity, which is utilized

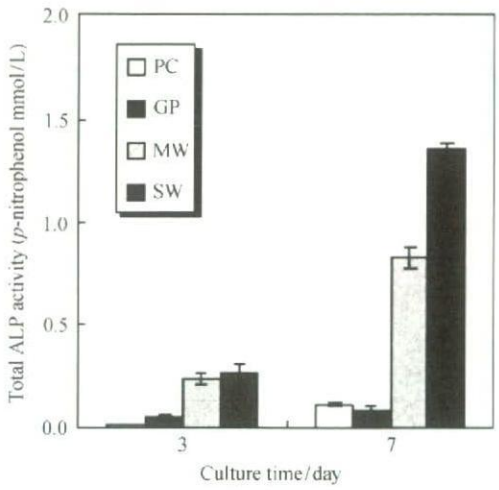

Fig. 8 Expression of total ALP activity from Saos2 cells cultured on the scaffolds of polycarbonate, graphite, MWCNT, and SWCNT, for 3 and 7 d [18]

for the application in artificial heart valve. By contrast, cell numbers and growth cultured on CNTs showed the characteristic behavior. Cell numbers proliferated on CNTs are much larger (Fig. 3). Osteoblast-like cell is usually grown in a spindle shape. On CNT scaffolds, cells are grown fully to the whole direction with numerous fine filopodia extended far from cell edge (Fig. 4) [18–20], which are mechanically combined with CNT meshwork. When tripsin, usually used to detach cells for cell number counting, was applied, cells were going to detach and float up, but could not be separated from the scaffold due to the mechanical binding of filopodia with CNTs [18]. All these results suggest the very good compatibility of CNTs to cells.

When CNTs are immersed in SBF, hydroxyapatite is precipitated [21,22]. This ~~work proves~~ the biocompatibility of CNTs as in the case of Ti.

However, one of the most influential factors to make a contrast difference in cell attachment and proliferation between graphite and CNTs would be the nonspecific affinity of CNTs to collagen, proteins, and also saccharides. Proliferated cell numbers are the largest on SWCNTs, followed by MWCNTs, and are very low on graphite (Fig. 3). This is in good agreement with the sequence in the results of the adsorbed amount of proteins (Fig. 7) and expression of ALP activity (Fig. 8). The culture medium contains various proteins including growth factors, which may affect the cell functions such as ALP activity, one of the markers of capability of new bone formation of osteoblasts. Therefore, the adsorption of proteins provides the favorable conditions to cells in the chemical or material aspects [18,23,24].

Another factor is the structural view point. Although CNTs generally have the tendency to agglomerate and form bundles, the wavy, fibrous agglomeration makes still a nano-meshwork conformation with a large porosity where cells can take nutrient elements or growth factors easily. In addition, the nanosize diameter of CNT fibers, a few to several tens nanometers, is close to that of filopodia of cells, which is about 100 nm. ~~And it~~ seems easy for the end of filopodia to interact with the CNT network. Tripsin is generally used for the detachment of cells from scaffold. On CNT scaffolds, however, cells cannot separate because of the mechanical binding of filopodia with the CNT network, which demonstrates the good cell adhesive properties of CNTs. All these would work for the excellent cell adhesion and growth on CNTs. Thus, CNTs could be the favorable materials for biomedical applications.

5 Conclusions

Graphite and CNTs, isomorphs of carbon composed of a similar graphene sheet crystal structure, showed a contrasting feature in cell attachment and proliferation, which is very low on graphite and excellent on CNTs. The affinity of CNTs to proteins leads to the high adsorption of proteins including growth factors in cell culture, which is responsible for excellent cell adhesion, growth, and its functional expression of ALP activity. In addition, the nano-meshwork structure of CNT agglomeration contributes physically to the favorite conditions for cell attachment. CNTs would work as scaffolds with the characteristic features.

Acknowledgements Research supported by Health and Labour Sciences Research Grants in Research on Chemical Substance Assessment of Ministry of Health, Labour and Welfare of Japan (H18-Chem-General-006).

References

1. Ushiro M, Uno K, Fujikawa T, et al. X-ray absorption fine structure (XAFS) analyses of Ni species trapped in graphene sheet of carbon nanofibers. Physical Review B: Condensed Matter, 2006, 73: 144103/1–11
2. Yokoyama A, Sato Y, Nodasaka Y, et al. Biological behavior of hat-stacked carbon nanofibers in the subcutaneous tissue in rats. Nano Letters, 2005, 5: 157–161
3. Sato Y, Shibata H, Kataoka S, et al. Strict preparation and evaluation of water-soluble hat-stacked carbon nanofibers for biomaedical application and their high biocompatibility: Influence of nanofiber-surface functional groups on cytotoxicity. Molecular Biosystems, 2005, 1: 142–145
4. Watari F, Tamura K, Yokoyama A, et al. Biochemical and pathological responses of cells and tissue to micro- and nanoparticles from titanium and other materials. In: Bauerlein E. Handbook of Biomineralization. Weinheim. Wiley-VCH, 2007, 3: 127–144
5. Kumazawa R, Watari F, Takashi N, et al. Effects of Ti ions and particles on cellular function and morphology of neutrophils. Biomaterials, 2002, 23: 3757–3764
6. Tamura K, Takashi N, Kumazawa R, et al. Effects of particle size on cell function and morphology in titanium and nickel. Materials

Transactions, 2002, 43: 3052–3057
7. Watari F, Inoue M, Akasaka T, et al. Comparison of morphology and behavior of carbon nanotubes and asbestos. Proceedings of the 6th Asian BioCeramics Symposium, 2006, 142–145
8. Kiura K, Sato Y, Yasuda M, et al. Activation of human monocytes and mouse splenocytes by single-walled carbon nanotubes. Journal of Biomedical Nanotechnology, 2005, 1: 359–364
9. Sato Y, Yokoyama A, Shibata K, et al. Influence of length on cytotoxicity of multi-walled carbon nanotubes against human acute monocytic leukemia cell line THP-1 *in vitro* and subcutaneous tissue of rats *in vivo*. Molecular BioSystems, 2005, 1: 176–182
10. Yokoyama A, Gelinsky M, Kawasaki T, et al. Biomimetic porous scaffolds with high elasticity made from mineralized collagen—an animal study. Journal of Biomedical Materials Research Part B Applied Biomaterials, 2005, 75B: 464–472
11. Gelinsky M, Bernhardt A, Eckert M, et al. Biomaterials based on mineralised collagen an artificial extracellular bone matrix. In: Watanabe M, Okuno O. Interface Oral Health Science. Japan. Springer, 2007, 323–328
12. Li X M, van Blitterswijk C A, Feng Q L, et al. The effect of calcium phosphate microstructure on bone-related cells *in vitro*. Biomaterials, 2008, 29: 3306–3316
13. Liao S, Wang W, Uo M, et al. A three-layered nano-carbonated hydroxyapatite/collagen/PLGA composite membrane for guided tissue regeneration. Biomaterials, 2005, 26: 7564–7571
14. Liao S, Watari F, Zhu Y, et al. The degradation of the three layered nano-carbonated hydroxyapatite/collagen/PLGA composite membrane *in vitro*. Dental Materials, 2007, 23: 1120–1128
15. Liao S, Xu G, Wang W, et al. Self-assembly of nano-hydroxyapatite on multi-walled carbon nanotubes. Acta Biomaterialia, 2007, 3: 669–675
16. Wang W, Watari F, Omori M, et al. Mechanical properties and biological behavior of carbon nanotube/polycarbosilane composites for implant materials. Journal of Biomedical Materials Research Part B Applied Biomaterials, 2007, 82: 223–230
17. Rosca I D, Watari F, Uo M, et al. Oxidation of multiwalled carbon nanotubes by nitric acid. Carbon, 2005, 43: 3124–3131
18. Aoki N, Akasaka T, Watari F, et al. Carbon nanotubes as scaffolds for cell and effect on cellular functions. Dental Materials Journal, 2007, 26: 178–185
19. Aoki N, Yokoyama A, Nodasaka Y, et al. Cell culture on a carbon nanotube scaffold. Journal of Biomedical Nanotechnology, 2005, 1: 402–405
20. Aoki N, Yokoyama A, Nodasaka Y, et al. Carbon nanotubes deposited on titanium implant for osteoblast attachment. Journal of Bionanoscience, 2007, 1: 14–16
21. Akasaka T, Watari F, Sato Y, et al. Apatite formation on carbon nanotubes. Materials Science and Engineering C, 2005, 26: 675–678
22. Akasaka T, Watari F. Nano-architechture on carbon nanotube surface by biomimetic coating. Chemistry Letters, 2005, 34: 826–827
23. Li X M, Gao H, Uo M, et al. Effect of carbon nanotubes on cellular functions *in vitro*. Journal of Biomedical Materials Research Part A, 2008, DOI: 10.1002/jbm.a.32203
24. Li X M, Gao H, Uo M, et al. Maturation of osteoblast-like Saos2 induced by carbon nanotubes. Biomedical Materials, 2009, DOI: 10.1008/17486041/4/1/015005